Available online at www.sciencedirect.com
ScienceDirect
Trans. Nonferrous Met. Soc. China 35(2025) 1691−1703
Transactions of Nonferrous Metals Society of China
www.tnmsc.cn

Kinetics of chalcopyrite dissolution in ammonia solution under sealed conditions and controlled redox potential

He-yun SUN[1,2,3,4], Ren-man RUAN[2,3], Jiu-shuai DENG[1,4]

1. Key Laboratory of Separation and Processing of Symbiotic-Associated Mineral Resources in Non-ferrous Metal Industry, Engineering Technology Research Center for Comprehensive Utilization of Rare Earth - Rare Metal - Rare Scattered in Non-ferrous Metal Industry, School of Chemical and Environmental Engineering, China University of Mining and Technology (Beijing), Beijing 100083, China;
2. National Engineering Research Center for Green Recycling of Strategic Metal Resources, Institute of Process Engineering, Chinese Academy of Sciences, Beijing 100190, China;
3. Key Laboratory of Green Process and Engineering, Institute of Process Engineering, Chinese Academy of Sciences, Beijing 100190, China;
4. Inner Mongolia Research Institute, China University of Mining and Technology (Beijing), Ordos 017001, China

Received 8 November 2024; accepted 10 April 2025

Abstract: To provide optimization strategies for chalcopyrite ammonia heap leaching processes, the key factors influencing chalcopyrite ammonia leaching kinetics were investigated under sealed reactor and controlled redox potential at ambient temperature. The results indicated that redox potential, particle size, and pH significantly affected chalcopyrite dissolution rates. The reaction orders with respect to particle size and hydroxyl ion concentration $c(OH^-)$ were determined to be −2.39 and 0.55, respectively. Temperature exhibited a marginal effect on chalcopyrite dissolution within the range of 25−45 °C. The ammonium carbonate medium proved more favorable for chalcopyrite leaching than ammonium chloride and ammonium sulfate systems. Surface deposits on the residues were identified as porous iron oxides, predominantly hematite and ferrihydrite, which produced diffusion barriers during leaching. Shrinking core model analysis revealed that the second stage of reaction was controlled by product-layer diffusion, which was further confirmed by the low activation energy (10.18 kJ/mol).

Key words: chalcopyrite; leaching kinetics; redox potential; ammoniacal leaching; surface deposits

1 Introduction

Chalcopyrite ($CuFeS_2$) is the most abundant copper-bearing mineral worldwide, accounting for 70% of global copper reserves [1,2]. However, it is also among the most refractory copper sulfides [3,4]. The traditional flotation−smelting process remains the preferred option for primary copper sulfides [5−7], while heap leaching has emerged as a viable alternative for low-grade sulfide copper ores and is widely applied for copper recovery from both low-grade copper oxides and secondary copper sulfides [6,8−10]. However, current heap leaching operations are predominantly conducted under acidic conditions [11−13], which are unsuitable for ores containing high concentrations of acid-consuming gangue minerals such as dolomite [14].

Corresponding author: Ren-man RUAN, Tel: +86-13701060670, E-mail: rmruan@126.com;
Jiu-shuai DENG, Tel: +86-18811172965, E-mail: jsdeng@cumtb.edu.cn
https://doi.org/10.1016/S1003-6326(25)66776-8

Consequently, the development of an alkaline-based heap leaching technology for chalcopyrite copper extraction has been anticipated in the mining industry.

The ammonia leaching process has been recognized as a promising method for copper recovery from primary copper sulfides associated with high acid-consuming gangue minerals, owing to its advantages of favorable leaching kinetics and high iron selectivity [15−18]. Extensive studies have been conducted on the ammoniacal leaching of chalcopyrite under oxidative conditions, focusing on leaching kinetics, reaction mechanisms, and surface deposits [19−25]. The reaction rate is predominantly controlled by surface chemical reactions [24,25]. Although both oxygen and Cu^{2+} are recognized as oxidants in this system, earlier studies primarily considered Cu^{2+} as a catalyst for chalcopyrite dissolution [24,25]. However, subsequent studies [26,27] have demonstrated that Cu^{2+} (rather than oxygen) serves as the dominant oxidant in ammoniacal systems, directly oxidizing chalcopyrite. This mechanism is supported by the stability of Cu^{+} in ammoniacal solutions, indicating that the Cu^{2+}/Cu^{+} redox couple can function as a redox mediator, oxidizing chalcopyrite more efficiently than dissolved oxygen [28].

The slow leaching kinetics of chalcopyrite is attributed to the formation of passivating iron oxyhydroxide surface films [29−33]. MOYO and PETERSEN [34] reported that an Fe-oxyhydroxide layer is formed during ammonium sulphate leaching. In contrast, only minimal iron deposition occurs on chalcopyrite surface in ammonia−ammonium carbonate systems, indicating that while the surface deposit layer influences the overall reaction, it does not passivate the mineral surface due to the amorphous and porous nature of the surface products. MA et al [27] identified the predominant iron species as amorphous hematite and six-line ferrihydrite in ammonium chloride solutions, which accounts for the observed dissolution retardation.

DUTRIZAC [35] explored the possibility of chalcopyrite heap leaching using ammonium carbonate solutions. The column leaching experiments were carried out on high-grade chalcopyrite ore (4.78% Cu, and particle size: 9.5−0.3 mm) at 25 °C. After two months of leaching with ammonia−ammonium carbonate solutions, a copper extraction rate of 20% was achieved, comparable to acid leaching results. It was suggested that chalcopyrite leaching kinetics was controlled by both chemical reactions and oxygen mass transfer. Notably, despite using covered solution reservoirs, significant ammonia losses (5%−20% of initial NH_3 input) occurred during the three-month leaching period, which may pose a significant challenge for industrial-scale implementation of ammonia-based chalcopyrite heap leaching. In parallel, NICOL [28] performed analogous column leaching experiments using ammonium chloride solutions for copper extraction from chalcopyrite ore. Their results demonstrated comparable efficiency to acid chloride leaching systems, while also exhibiting significant ammonia volatilization losses. These findings conclusively identified ammonia losses as “the most critical techno-economic barrier hindering commercial-scale implementation of ammoniacal chalcopyrite heap leaching”.

Previous studies on ammonia heap leaching were conducted in open systems, where significant ammonia volatilization limited the commercial application. To address this, the authors developed a fully enclosed ammonia heap leaching technology that virtually eliminates ammonia volatilization [36]. However, efficient chalcopyrite leaching under closed conditions poses another challenge. This study systematically investigates critical parameters governing chalcopyrite leaching kinetics under closed conditions, including redox potential, ammonium salts selection, particle size, pH, and temperature. Furthermore, we also characterize surface products on residues and evaluate their passivation effects, aiming to provide optimization strategies for industrial operations of chalcopyrite ammonia heap leaching.

2 Experimental

2.1 Chalcopyrite sample

The chalcopyrite samples used in this investigation were sourced from Hezhang County, Guizhou Province, China. Following crushing and grinding, the material was wet-screened using anhydrous ethanol to produce five size fractions: ≤25, 25−46, 46−74, 74−105, and ≥105 μm. The chemical composition of each size fraction is given in Table 1. The results revealed no significant differences in the contents of Cu and Fe elements

among the different size fractions. Notably, the ≤25 μm fraction exhibited a Cu/Fe ratio of 1.14, matching the theoretical stoichiometric value, while coarser fractions showed marginally lower ratios, suggesting surface copper depletion. XRD characterization (Fig. 1) confirmed chalcopyrite as the dominant crystalline phase, in agreement with prior literature reports [37].

2.2 Leaching experiments

To maintain ammonia stability and minimize volatilization, leaching experiments were conducted in sealed 1000 mL flasks containing 700 mL of ammonium salt solution with a total ammonia concentration (NH_4^++NH_3) of 2 mol/L. The system was supplemented with 1 g/L Cu^{2+} as $CuSO_4·5H_2O$. To ensure continuous copper leaching under sealed conditions, a potential-controlled method was employed to add hydrogen peroxide to the solution, oxidizing Cu^+ to regenerate the Cu^{2+} oxidant. The redox potential (ORP) of the leaching solution was controlled at (50±5) mV (vs Ag/AgCl) using an automated control system consisting of an ORP electrode, controller, and peristaltic pump for H_2O_2 dosing (Fig. 2). Solution pH was adjusted between 7.5 and 9.5 in 0.5 pH unit increments by adding 10 mol/L NaOH into $(NH_4)_2SO_4$ solutions, and the temperature was controlled between 25 and 45 °C in 5 °C intervals using an oil bath with a magnetic stirrer. Comparative tests were performed with $(NH_4)_2CO_3$, NH_4Cl and $(NH_4)_2SO_4$ to evaluate the effects of different ammonium salts on leaching kinetics. The particle size effect was investigated using five classified fractions: ≤25 μm, 25−46 μm, 46−74 μm, 74−105 μm, and ≥105 μm.

Table 1 Chemical composition of chalcopyrite particle size fractions

Size fraction/μm	*w*(Cu)/wt.%	*w*(Fe)/wt.%	Cu/Fe ratio
≤25	35.67	31.34	1.14
25−46	32.95	30.05	1.10
46−74	32.94	30.87	1.07
74−105	32.58	29.69	1.10
≥105	34.40	31.20	1.10

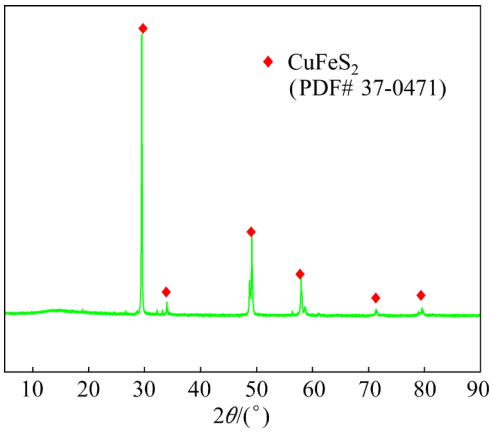

Fig. 1 X-ray diffraction pattern of chalcopyrite (≤25 μm particle size fraction)

The 5 g of chalcopyrite samples were added to each flask and leached with magnetic stirring at 500 r/min for 6 h. During leaching, 2 mL aliquots were periodically collected for copper concentration analysis using a Puxi A3 atomic absorption spectroscopy (AAS), with immediate replenishment of equal-volume fresh leaching solution to maintain constant liquid level.

Following the leaching experiment, solid residues were collected by vacuum filtration through a 0.25 μm microporous membrane. The filter cake was sequentially rinsed with: (1) a dilute ammonium salt solution and (2) deionized water to remove residual lixiviant. Subsequently, purified residues were lyophilized at −50 °C for 24 h in a freeze dryer.

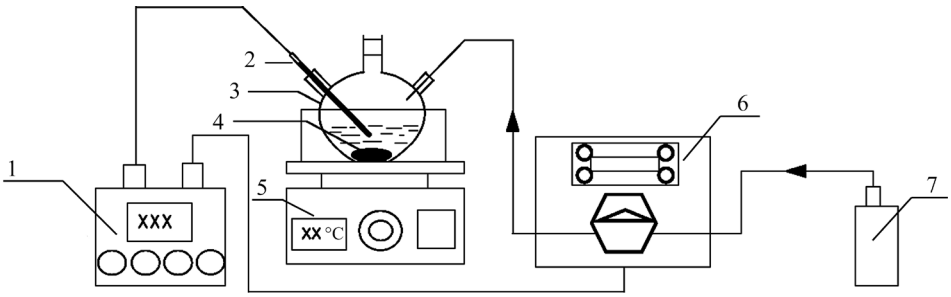

Fig. 2 Schematic diagram of experimental setup with integrated temperature and ORP control systems: 1−ORP controller; 2−ORP electrode; 3−Three-neck round-bottom flask; 4−Magnetic stir bar; 5−Magnetic stirrer with oil bath; 6−Peristaltic pump; 7−Hydrogen peroxide reservoir

2.3 Surface characterization

2.3.1 SEM−EDS analysis

Sample surfaces were sputter-coated with gold prior to analysis. Microstructural characterization was performed using a field-emission SEM (JSM−7610F, JEOL, Japan) equipped with an EDS detector (ULTIM MAX, Oxford Instruments) at an accelerating voltage of 15 kV.

2.3.2 Raman spectroscopy

Raman spectra were acquired using a Renishaw inVia Reflex confocal Raman microscope equipped with a 514 nm argon-ion laser. The system was calibrated with a silicon reference (520.5 cm^{-1}) prior to measurements. To prevent laser-induced sample damage, the power density was maintained at 0.3 mW throughout analyses, with each spectrum representing four 60 s accumulations. Spectral data were collected across 150−2000 cm^{-1} wavenumber range.

3 Results and discussion

3.1 Effect of redox potential

Hydrogen peroxide was added to an ammonium salt solution to maintain a constant solution potential. This approach was adopted to compare the effects of controlled vs uncontrolled potential on the kinetics of chalcopyrite ammonia leaching under anoxic conditions. The experiments were conducted in a 1 mol/L $(NH_4)_2CO_3$ solution containing 1 g/L Cu^{2+}, at pH of 9, with a particle size of ≤25 μm and a temperature of 30 °C.

In the ammoniacal system, Cu^{2+} was identified as the primary oxidant for chalcopyrite (Reaction (2)), rather than molecular oxygen (Reaction (1)). Cu^{2+} directly oxidizes chalcopyrite, which is attributable to the stability of Cu^{+} in ammoniacal solutions, allowing the Cu^{2+}/Cu^{+} couple to function as an effective redox mediator. This mediation results in faster chalcopyrite oxidation compared to dissolved oxygen. The enhanced leaching kinetics by Cu^{2+} could be explained by its higher reactivity and solubility relative to dissolved O_2, as well as the rapid regeneration of Cu^{2+} through the oxidation of Cu^{+} by dissolved O_2 (Reaction (3)) [26,27]:

$$2CuFeS_2+8.5O_2+8NH_3+4OH^-=\!=2Cu(NH_3)_4^{2+}+Fe_2O_3+4SO_4^{2-}+2H_2O \quad (1)$$

$$2CuFeS_2+32Cu(NH_3)_4^{2+}+38OH^-=\!=34Cu(NH_3)_2^{+}+Fe_2O_3+4SO_4^{2-}+60NH_3+19H_2O \quad (2)$$

$$4Cu(NH_3)_2^{+}+8NH_3+O_2+2H_2O=\!=4Cu(NH_3)_4^{2+}+4OH^- \quad (3)$$

It was reported that $[Cu(NH_3)_4^{2+}]/[Cu(NH_3)_2^{+}]$ ratio is directly proportional to the system's redox potential (E_h) of the system [38]. Equation (4) was proposed to describe this relationship, which shows that under constant ammonia concentration, E_h increases as the $[Cu(NH_3)_4^{2+}]/[Cu(NH_3)_2^{+}]$ ratio increases:

$$E_h=0.074-0.1182\lg[NH_3]+0.0591\lg\frac{[Cu(NH_3)_4^{2+}]}{[Cu(NH_3)_2^{+}]} \quad (4)$$

Their findings demonstrate that chalcopyrite leaching under anoxic and sealed conditions could be achieved through addition of oxidants such as hydrogen peroxide to regenerate Cu^{2+} and increase the solution redox potential (E_h).

As shown in Fig. 3, the redox potential (E_h) of the leaching solution significantly affects the chalcopyrite leaching rate under sealed conditions, consistent with the findings of MA et al [27]. With hydrogen peroxide addition to the ammonium carbonate solution, the E_h increased and stabilized at (50±5) mV (vs Ag/AgCl), resulting in a 52% copper extraction yield within 6 h. In contrast, under uncontrolled potential conditions (without H_2O_2 addition), E_h rapidly dropped to –(30±5) mV (vs Ag/AgCl) within 1 h because Cu^{2+} was completely consumed without oxidant-driven regeneration of Cu^{+} to Cu^{2+}. At this low E_h of –(30±5) mV, only 18% copper was dissolved, significantly lower than that (52%) at controlled E_h ((50±5) mV).

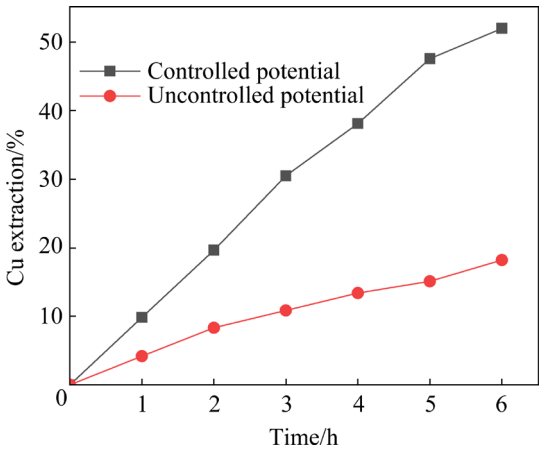

Fig. 3 Copper extraction from chalcopyrite under sealed conditions at controlled potential of (50±5) mV (vs Ag/AgCl) and uncontrolled potential of –(30±5) mV (vs Ag/AgCl)

The contents of Cu and Fe in the residues were analyzed and are shown in Table 2. The Cu extraction reached 52.24% and 19.00%, consistent with solution analysis results. The decreased Cu/Fe ratio in the residues indicates the formation of a copper-deficient, iron-rich surface layer. During the ammonia leaching process, Cu dissolved while Fe accumulated on the chalcopyrite surface (according to Reactions (1) and (2)).

Table 2 Contents of copper (Cu) and iron (Fe) in residues and copper extraction under controlled and uncontrolled potentials

Sample	Content/wt.%		Cu/Fe ratio	Cu extraction/%	
	Cu	Fe		From residue	In solution
Feed	35.67	31.34	1.14	–	–
Residue under controlled redox	22.74	35.98	0.63	52.24	51.95
Residue under uncontrolled redox	32.15	30.84	1.04	19.00	18.20

3.2 Effect of ammonium salts

Figure 4 shows copper dissolution from chalcopyrite in various ammonium salt solutions under sealed conditions. The test conditions were: total ammonia (NH_4^++NH_3) 2 mol/L, Cu^{2+} 1 g/L , pH 9, temperature 30 °C, particle size ≤25 μm, and redox potential (50±5) mV (vs Ag/AgCl). In the ammonium chloride system, the copper leaching rate initially increased rapidly before gradually decreasing, achieving 42.21% extraction yield within 6 h. In contrast, ammonium sulfate system showed slower kinetics, with only 39.9% copper extraction in the same period. The ammonium carbonate system exhibited nearly linear leaching kinetics, reaching the highest extraction yield of 52.2% after 6 h.

Chemical analysis of the leaching residues confirmed that the copper extraction yield determined from the residues matched that measured in the solution (Table 3). The Cu/Fe ratio (0.69±0.06) was significantly lower than the theoretical stoichiometric value of 1.14, confirming iron enrichment as a surface layer (likely iron oxyhydroxides) with preferential copper dissolution into the ammoniacal solution. Notably, the ammonium carbonate system enabled higher copper dissolution compared to the ammonium sulfate and chloride systems. This enhancement likely resulted from iron carbonate complexation, which modified the iron deposit morphology and inhibited passivation layer formation. These findings align with the mechanism proposed by MOYO and PETERSEN [34].

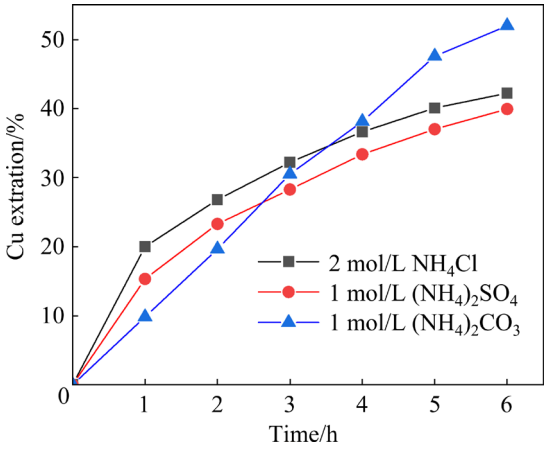

Fig. 4 Copper extraction from chalcopyrite in different ammonium salt solutions

Table 3 Contents of copper (Cu) and iron (Fe) in residues and copper extraction for various ammonium salt solutions

Ammonium salt	Content/wt.%		Cu/Fe ratio	Cu extraction/%	
	Cu	Fe		From residue	In solution
$(NH_4)_2SO_4$	26.93	36.14	0.75	37.16	39.9
NH_4Cl	23.41	36.28	0.65	47.99	42.21
$(NH_4)_2CO_3$	22.74	35.98	0.63	52.24	51.95

3.3 Effect of particle size

The effect of particle size on chalcopyrite dissolution was investigated under the sealed conditions at a controlled potential of (50±5) mV (vs Ag/AgCl), 30 °C, in 1 mol/L $(NH_4)_2CO_3$ solution containing 1 g/L Cu^{2+}, at pH 9 with 500 r/min agitation. As shown in Fig. 5, copper extraction rates increased significantly with decreasing particle size below 46 μm, whereas size variations showed negligible effects for coarser particles (>46 μm). These results are consistent with the 44 μm threshold for copper concentrate leaching reported by NABIZADEH and AGHAZADEH [21].

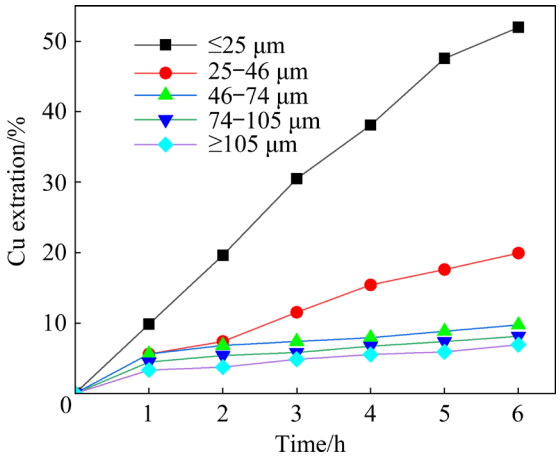

Fig. 5 Copper extraction from chalcopyrite with different particle size fractions

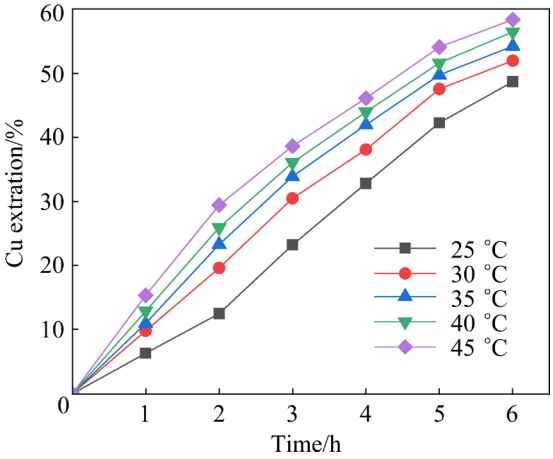

Fig. 6 Copper extraction from chalcopyrite at different temperatures (25−45 °C)

The Cu and Fe contents in the residues were analyzed, as shown in Table 4. The copper extraction calculated from the residues is consistent with that obtained from the solution analysis. A decrease in the Cu/Fe ratio was observed with increasing copper extraction.

Table 4 Cu and Fe contents in residues and copper extraction for different particle size fractions

Particle size/μm	Content/wt.%		Cu/Fe ratio	Cu extraction/%	
	Cu	Fe		From residue	In solution
≥105	35.28	32.35	1.090	6.34	6.91
74−105	31.50	32.13	1.086	8.85	8.11
46−74	32.78	32.92	1.041	10.04	9.73
25−46	32.36	32.32	0.970	19.10	19.92
≤25	22.74	35.98	0.63	52.24	51.95

3.4 Effect of temperature

Given that most heap leaching operations proceed at ambient temperatures (typically 10−40 °C), copper dissolution was investigated from 25 to 45 °C under sealed conditions at a controlled potential of (50±5) mV (vs Ag/AgCl) in 1 mol/L $(NH_4)_2CO_3$ solution (1 g/L Cu^{2+}, pH 9, 500 r/min, ≤25 μm). As shown in Fig. 6, although copper extraction increased with temperature, its effect on chalcopyrite leaching kinetics remained marginal. These findings agree with observations reported by NABIZADEH and AGHAZADEH [21], who noted comparable temperature insensitivity (25−60 °C, ≤25 μm particles).

3.5 Effect of pH

Chalcopyrite leaching was investigated at varying pH (7.5−9.5, adjusted with NaOH or H_2SO_4) under sealed conditions at a controlled potential of (50±5) mV (vs Ag/AgCl), 30 °C, in 1 mol/L $(NH_4)_2SO_4$ solution containing 1 g/L Cu^{2+}, with 500 r/min agitation and particle size ≤25 μm. As shown in Fig. 7, the leaching rate increased exponentially with pH, showing a threefold enhancement from pH 7.5 to 9.5. This pH dependence aligns with observations by BECKSTEAD and MILLER [24] and NABIZADEH and AGHAZADEH [21] in ammoniacal systems.

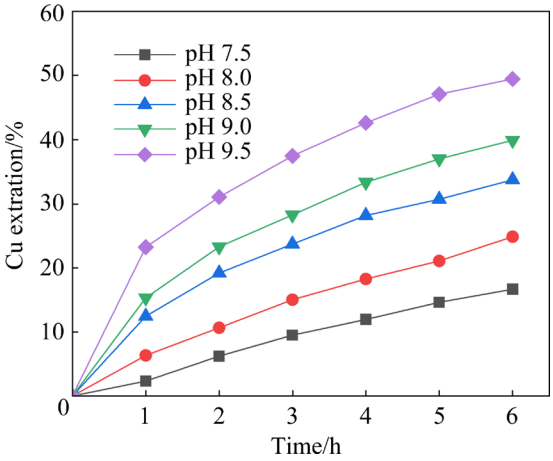

Fig. 7 Copper extraction from chalcopyrite at different pH (7.5−9.5)

3.6 SEM and EDS analysis results

SEM−EDS characterization of leaching residues revealed distinct surface morphologies in different ammonium salt systems (Fig. 8, and

Table 5). Dense passivation layers were formed in ammonium chloride and ammonium sulfate solutions (Figs. 8(a, b)), whereas ammonium carbonate solutions produced porous corrosion layers (Fig. 8(c)). These morphological differences explain the enhanced leaching kinetics in carbonate media, as the porous structure facilitates reagent diffusion [39]. Mechanistic analysis suggests that (1) in carbonate systems, soluble Fe(II)−CO_3 complexes prevent surface precipitation, maintaining reaction interfaces, and (2) sulfate systems favor iron sulfate precipitation, forming diffusion-barrier layers [34]. These findings demonstrate how anion selection dictates surface reaction pathways.

Energy-dispersive spectroscopy (EDS) results for the newly exposed surface at Spot 15 revealed a composition of 26.82% Cu, 22.00% Fe, 43.82% S, and 7.37% O, matching the pristine chalcopyrite composition. EDS analysis of the surface deposit (Spot 17) from ammonium chloride leaching indicated a composition of 15.54% Cu, 22.71% Fe, 32.64% S, and 29.10% O, showing comparable composition to Spot 20 in ammonium sulfate. The atomic percentages yield Cu/Fe and S/Fe ratios of 0.68 and 1.43, respectively, which were significantly lower than the 1:1 and 2:1 ratios of stoichiometric chalcopyrite ($CuFeS_2$), evidencing preferential dissolution of copper and sulfur with iron accumulation as oxyhydroxides. For the ammonium carbonate system, the analysis showed a composition of 6.46% Cu, 27.90% Fe, 27.22% S, and 38.42% O. The resultant Cu:Fe:S:O ratio

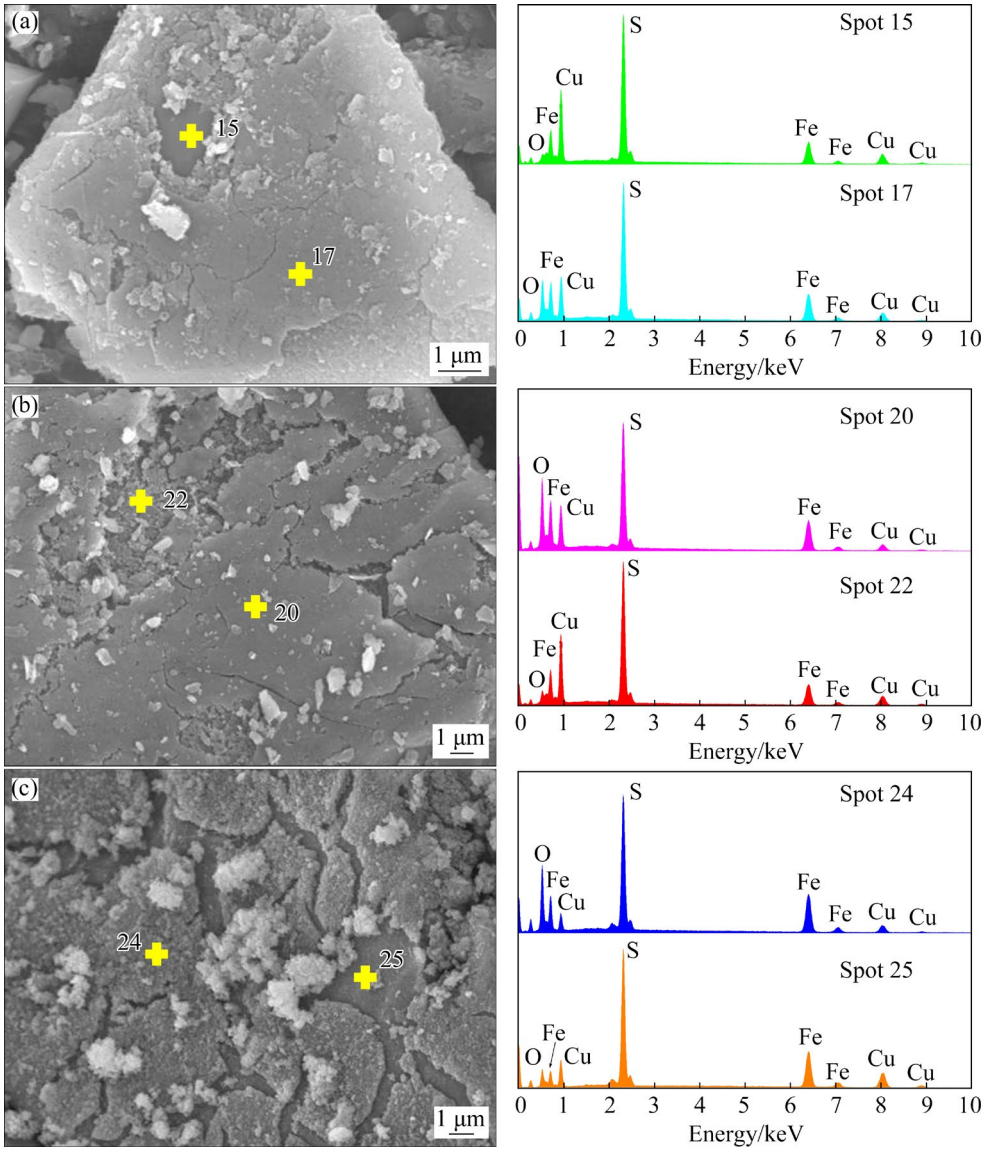

Fig. 8 SEM images and EDS analysis results of leached residues in different ammonium salt solutions: (a) Ammonium chloride; (b) Ammonium sulfate; (c) Ammonium carbonate

Table 5 EDS analysis results of leached residues

Ammonium salt	Spot	Composition/at.%				Cu/Fe ratio	S/Fe ratio
		Cu	Fe	S	O		
Ammonium chloride	15	26.82	22.00	43.82	7.37	1.22	1.99
	17	15.54	22.71	32.64	29.10	0.68	1.43
Ammonium sulfate	20	13.39	21.14	25.55	39.91	0.63	1.21
	22	25.40	21.21	41.77	11.63	1.20	1.97
Ammonium carbonate	24	6.46	27.90	27.22	38.42	0.23	0.98
	25	12.83	34.69	37.62	14.85	0.37	1.08

(1:4:4:6) confirmed iron oxyhydroxide precipitation post-dissolution, consistent with solution pH>8.5 promoting $Fe(OH)_3$ formation, and carbonate complexation inhibiting Fe^{3+} redeposition [34].

3.7 Raman spectroscopy results

To identify the composition of surface reaction products, Raman spectroscopic analysis (514 nm laser, 0.3 mW) was performed on both the feed and leached chalcopyrite in various ammonium salt solutions (NH_4Cl/$(NH_4)_2SO_4$/$(NH_4)_2CO_3$). Figure 9 shows the Raman spectra of both the feed and leached chalcopyrite. The feed chalcopyrite exhibited characteristic vibrational modes at 292, 324, and 356 cm^{-1}, corresponding to fundamental Cu—Fe—S lattice vibrations [27]. After leaching in various ammonium salts, these primary peaks persisted while new features emerged at 224, 409, 610, and 1321 cm^{-1} (two-magnon scattering) in all residues. These additional peaks were diagnostically assigned to hematite (α-Fe_2O_3) surface deposition [40] based on (1) the 1321 cm^{-1} two-magnon scattering unique to hematite, (2) the characteristic 224−409 cm^{-1} Fe — O vibrational modes, and (3) our EDS results showing iron enrichment (Section 3.6).

Additionally, the broad 600−750 cm^{-1} envelope corresponds to six-line ferrihydrite ($5Fe_2O_3·9H_2O$) [27,29,41], as evidenced by (1) characteristic peak broadening (FWHM > 50 cm^{-1}), and (2) absence of crystalline goethite signatures. These findings align with established mechanisms of chalcopyrite oxidative dissolution in ammoniacal media, where Fe_2O_3 phases dominate in the surface products [27,42−44]. The combined Raman−EDS results demonstrate an anion-dependent surface passivation process, with carbonate systems showing distinct ferrihydrite/hematite ratios (Table 5).

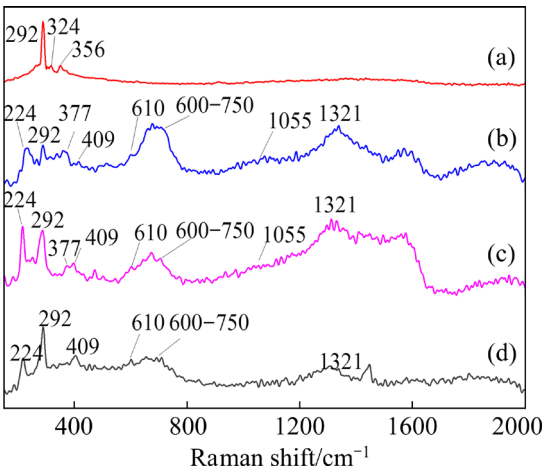

Fig. 9 Raman spectra of chalcopyrite in feed (a), and after leaching in NH_4Cl (b), $(NH_4)_2SO_4$ (c), and $(NH_4)_2CO_3$ (d) solutions

Raman analysis revealed two key findings regarding sulfur speciation: (1) Absence of elemental sulfur (no characteristic S^0 vibrational modes at 153 and 219 cm^{-1} were detected), confirming complete sulfur oxidation under these conditions; (2) Tetrathionate ($S_4O_6^{2-}$) formation, with two distinct peaks observed at 377 cm^{-1} (ν_s: S—S stretching) and 1050 cm^{-1} (ν_{as}: S—O stretching) in all systems except the ammonium carbonate solution. These features were conclusively assigned to tetrathionate ($S_4O_6^{2-}$) formation based on excellent agreement with reference $Na_2S_4O_6$ spectra [27,45].

Electrochemical analyses confirm that Cu^{2+} mediates the oxidation of thiosulfate ($S_2O_3^{2-}$) to tetrathionate ($S_4O_6^{2-}$) [46], indicating that $S_2O_3^{2-}$ is the initial product of chalcopyrite oxidation. This reaction pathway of chalcopyrite oxidation

proceeds through a thiosulfate intermediate mechanism rather than direct oxidation to sulfate, as evidenced by (1) the presence of tetrathionate ($S_4O_6^{2-}$) during ammoniacal leaching, (2) thermodynamic calculations predicting $S_2O_3^{2-}$ as the dominant intermediate in ammoniacal solutions at pH 7−9 [17], (3) electrochemical measurements showing $S_2O_3^{2-}$ stability below 0.6 V [18], and (4) synchrotron XANES spectra confirming the presence of $S_2O_3^{2-}$ during initial oxidation [24].

3.8 Kinetic analysis

The leaching kinetics of chalcopyrite in oxidative ammoniacal solutions were analyzed using the shrinking core model (SCM) [47,48]. This model describes two possible rate-limiting mechanisms: (1) surface chemical reaction control (Eq. (5)) and (2) product-layer diffusion control (Eq. (6)):

$$1-(1-x)^{1/3}=k_C t \quad (5)$$

$$1+2(1-x)-3(1-x)^{2/3}=k_D t \quad (6)$$

where x is the fraction of dissolved Cu; t is time; k_C and k_D are the apparent rate constants for reaction and diffusion, respectively.

The apparent activation energy (E_a) was determined using Arrhenius equation (7) [49,50]:

$$k=A\exp[-E_a/(RT)] \quad (7)$$

where k is apparent rate constant, A is frequency factor, R is molar gas constant and T is thermodynamic temperature.

The temperature-dependent leaching profiles (Fig. 6) revealed biphasic kinetics: a rapid initial dissolution phase (0−2 h) followed by a slower secondary phase (2−6 h). This kinetic transition aligns with the progressive formation of a passivating product layer, as evidenced by SEM−EDS analysis (Fig. 8).

Kinetic modeling using Eqs. (5) and (6) (Table 6, and Figs. 10(a, b)) identifies two distinct rate-limiting mechanisms: (1) The initial phase (0−2 h) was controlled by chemical reactions; (2) The later phase (2−6 h) was controlled by diffusion through the product layer.

The Arrhenius plots (Figs. 10(c, d)) further confirmed this mechanistic transition, showing a characteristic decrease in activation energy from 33.89 kJ/mol (chemical control) to 10.18 kJ/mol (diffusion control) for such passivation systems.

The rate constants (k) and correlation coefficients (R^2) for particle size and hydroxyl ion concentration ($c(OH^-)$) were determined using Eqs. (5) and (6), as summarized in Table 7. Key parameters were derived through the following procedures: (1) $c(OH^-)$ was calculated from pH measurements using the ionic product of water ($K_W=1.0\times10^{-14}$); (2) Particle sizes represent the mean values of each size fraction.

Kinetic analysis showed that the diffusion-controlled models exhibited higher R^2 values compared to chemical reaction models, confirming product-layer diffusion as the rate-limiting step in ammoniacal solutions.

The reaction orders obtained from ln k_D versus ln D_0 and ln $c(OH^-)$ plots (Fig. 11) were −2.39 for particle size and 0.55 for $c(OH^-)$. These results align with the established studies: (1) The negative

Table 6 Kinetic parameters derived from temperature-varied leaching experiments

Reaction stage	$1-(1-x)^{1/3}$			$1+2(1-x)-3(1-x)^{2/3}$		
	k_C/h^{-1}	Correlative coefficient, R^2	$E_a/(kJ\cdot mol^{-1})$	k_D/h^{-1}	Correlative coefficient, R^2	$E_a/(kJ\cdot mol^{-1})$
Initial phase (0−2 h)	0.022	1.000	33.89	0.0025	0.907	−
	0.035	1.000		0.006	0.900	
	0.042	0.996		0.009	0.879	
	0.047	0.999		0.011	0.894	
	0.055	1.000		0.015	0.910	
Later phase (2−6 h)	0.039	0.998	−	0.025	0.981	10.18
	0.037	0.991		0.028	0.989	
	0.037	0.991		0.029	0.997	
	0.037	0.995		0.031	0.997	
	0.037	0.994		0.033	0.995	

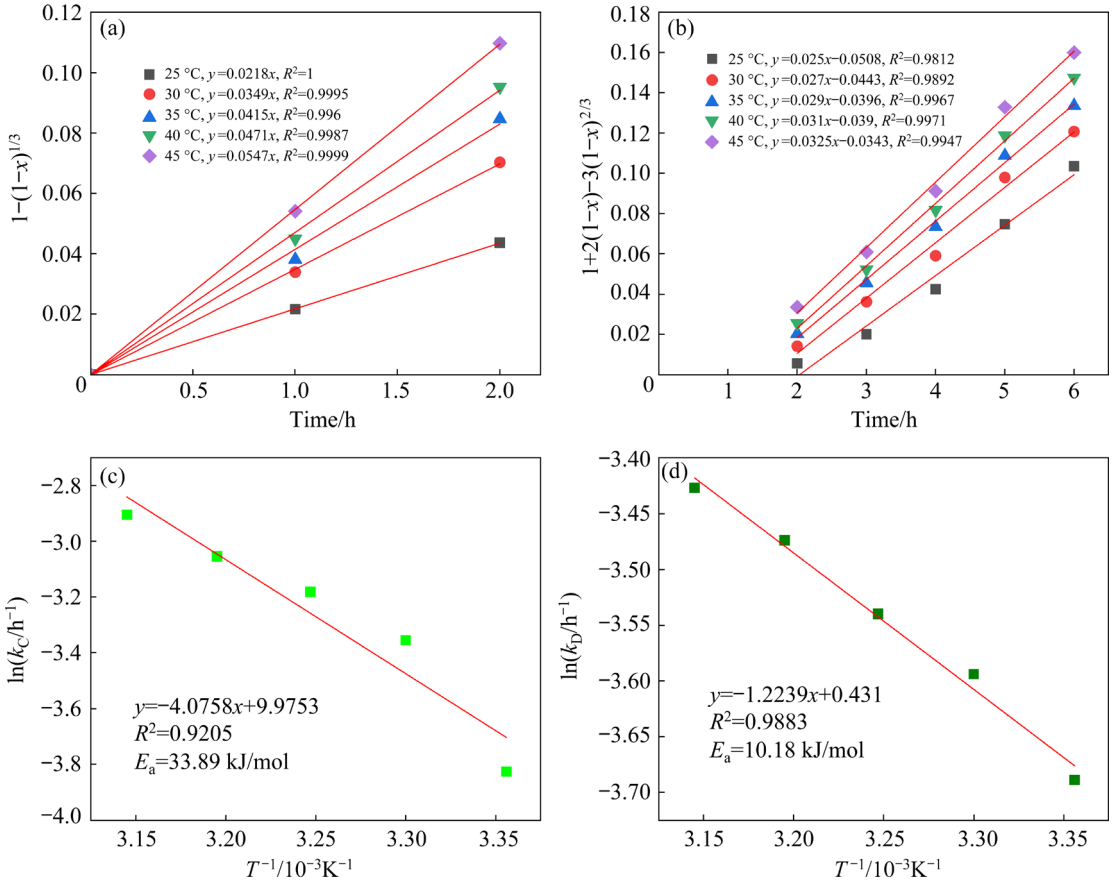

Fig. 10 Kinetic analysis of chalcopyrite leaching: (a) Plot of $1-(1-x)^{1/3}$ vs time (0−2 h) for chemical reaction-controlled stage; (b) Plot of $1+2(1-x)-3(1-x)^{2/3}$ vs time (2−6 h) for diffusion-controlled stage; (c) Arrhenius plot (ln k vs $1/T$) for initial stage (chemical reaction control, E_a=33.89 kJ/mol); (d) Arrhenius plot for later stage (diffusion control, E_a=10.18 kJ/mol)

Table 7 Apparent rate constants (k), correlation coefficients (R^2), and reaction orders with respect to particle size (D_0) and hydroxyl ion concentration ($c(OH^-)$)

Parameter		$1-(1-x)^{1/3}$		$1+2(1-x)-3(1-x)^{2/3}$		Reaction order
		k_C/h^{-1}	R^2	k_D/h^{-1}	R^2	
Particle size/μm	20	0.037	0.997	0.018	0.898	−2.39
	35.5	0.013	0.980	0.002	0.929	
	60	0.007	0.548	0.001	0.922	
	89.5	0.005	0.628	0.000	0.961	
	105.5	0.004	0.768	0.000	0.982	
Hydroxyl ion concentration/(mol·L^{-1})	$10^{-6.5}$	0.010	0.994	0.001	0.910	0.55
	10^{-6}	0.016	0.980	0.003	0.937	
	$10^{-5.5}$	0.024	0.889	0.007	0.995	
	10^{-5}	0.030	0.886	0.011	0.996	
	$10^{-4.5}$	0.040	0.821	0.019	0.997	

particle size dependence (−2.39) matches the nano-porous diffusion barriers reported by NABIZADEH and AGHAZADEH [21]; (2) The sub-linear $c(OH^-)$ dependence (0.55) corresponds to the surface protonation model proposed by BECKSTEAD and MILLER [24].

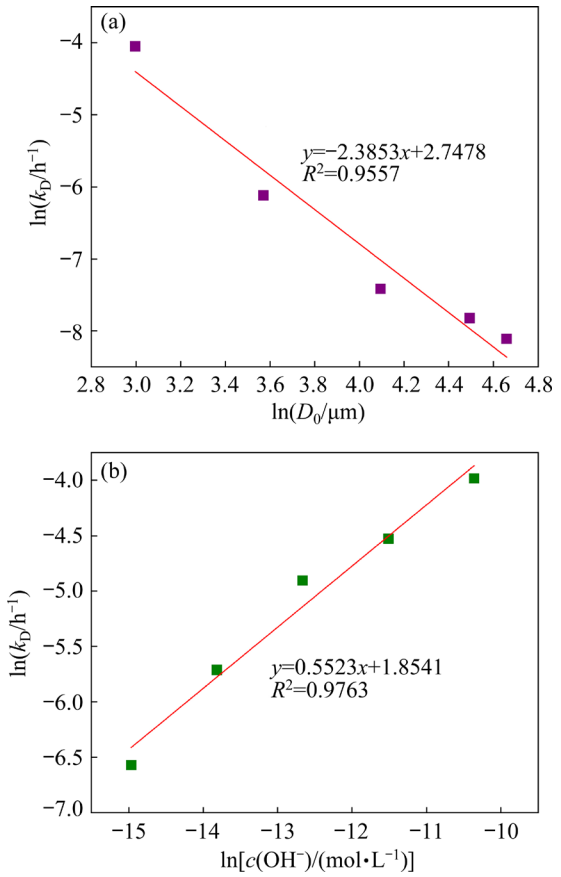

Fig. 11 Dependence of leaching kinetics on particle size (ln k_D vs ln D_0) (a) and hydroxyl ion concentration (ln k_D vs ln $c(OH^-)$) (b)

4 Conclusions

(1) The leaching kinetics of chalcopyrite exhibited strong dependence on redox potential. Under controlled potential conditions ((50±5) mV vs Ag/AgCl), copper extraction reached 52.2% within 6 h, representing a 2.9-fold enhancement compared with that under uncontrolled potential of −(30±5) mV (18.0% extraction).

(2) The chalcopyrite leaching kinetics demonstrated strong dependence on both particle size and solution pH, with experimentally determined reaction orders of −2.39 for particle size and 0.55 for hydroxyl ion concentration ($c(OH^-)$). In contrast, temperature variations (25−45 °C) showed negligible impact. Notably, comparative leaching tests revealed that the ammonium carbonate system achieved 9%−12% higher extraction efficiency than the chloride or sulfate systems.

(3) During the leaching process, a thick and porous layer was formed on chalcopyrite surface. SEM−EDS and Raman analyses confirmed that this layer consisted predominantly of hematite (α-Fe_2O_3) and disordered ferrihydrite ($5Fe_2O_3·9H_2O$), which collectively functioned as a diffusion barrier.

(4) Kinetic analysis revealed a distinct two-stage mechanism: the initial stage (0−2 h) was primarily controlled by chemical reactions (R^2>0.99, E_a=33.89 kJ/mol); the later stage (2−6 h) was controlled by diffusion through the product layer (R^2 > 0.98, E_a=10.18 kJ/mol).

CRediT authorship contribution statement

He-yun SUN: Investigation, Methodology, Software, Data curation and analysis, Writing − Original draft; **Ren-man RUAN:** Supervision, Resources, Validation, Writing − Review & editing, Project administration, Funding acquisition; **Jiu-shuai DENG:** Supervision, Validation, Writing − Review & editing, Project administration.

Declaration of competing interest

The authors declare that they have no known competing financial interests or personal relationships that could have appeared to influence the work reported in this paper.

Acknowledgments

The authors are grateful for the financial supports from the Strategic Priority Research Program of Chinese Academy of Sciences (No. XDA0430304).

References

[1] WANG Shi-jie. Copper leaching from chalcopyrite concentrates [J]. JOM, 2005, 57: 48−51.

[2] OWEN N D, RAM R, VOLLERT L, SEAMAN B, ETSCHMANN B, XING Yan-lu, ROSEMANN M, VERDUGO L, O'CALLAGHAN J, BRUGGER J. The deleterious role of gangue mineralogy in copper extraction: A case study of poor recovery in leaching low-grade Cu ores [J]. Applied Geochemistry, 2024, 166: 105984.

[3] BARTON I F, HISKEY J B. Chalcopyrite leaching in novel lixiviants [J]. Hydrometallurgy, 2022, 207: 105775.

[4] PADILLA R, VEGA D, RUIZ M C. Pressure leaching of sulfidized chalcopyrite in sulfuric acid–oxygen media [J]. Hydrometallurgy, 2007, 86: 80−88.

[5] KOLEINI S M J, JAFARIAN M, ABDOLLAHY M, AGHAZADEH V. Galvanic leaching of chalcopyrite in atmospheric pressure and sulphate media: Kinetics and surface studies [J]. Industrial & Engineering Chemistry Research, 2010, 49(13): 5997−6002.

[6] DOMIC E M. A review of the development and current status of copper bioleaching operations in Chile: 25 years of successful commercial implementation [M]//Biomining.

Springer, 2007, 81−95.
[7] VALENTA R K, KEMP D, OWEN J R, CORDER G D, LÈBRE É. Re-thinking complex orebodies: Consequences for the future world supply of copper [J]. Journal of Cleaner Production, 2019, 220: 816−826.
[8] PETERSEN J. Heap leaching as a key technology for recovery of values from low grade ores—A brief overview [J]. Hydrometallurgy, 2016, 165: 206−212.
[9] WATLING H R. The bioleaching of sulphide minerals with emphasis on copper sulphides — A review [J]. Hydrometallurgy, 2006, 84: 81−108.
[10] BRIERLEY J A, BRIERLEY C L. Present and future commercial applications of biohydrometallurgy [J]. Hydrometallurgy, 2001, 59: 233−239.
[11] DREISINGER D. Copper leaching from primary sulfides: Options for biological and chemical extraction of copper [J]. Hydrometallurgy, 2006, 83: 10−20.
[12] PRADHAN N, NATHSARMA K C, RAO K S, SUKLA L B, MISHRA B K. Heap bioleaching of chalcopyrite: A review [J]. Minerals Engineering, 2008, 21(5): 355−365.
[13] SRACEK O, ETTLER V, MARTIN M, KŘÍBEK B, MAPANI B, PENÍŽEK V, ZÁDOROVÁ T, VANĚK A. Identification of processes in Cu-ore heap leaching using Cu isotopes and leachate chemistry at Tschudi Mine, northern Namibia [J]. Hydrometallurgy, 2024, 228: 106356.
[14] THOMAS M. Understanding gangue acid consumption in copper sulfide heap leaching: predicting the impact of carbonates, silicates and secondary precipitates [J]. Minerals Engineering, 2021, 171: 107090.
[15] WANG Xi, CHEN Qi-yuan, YIN Zhou-lan, HU Hui-ping, XIAO Zhong-liang. Real-solution stability diagrams for copper−ammonia−chloride−water system [J]. Journal of Central South University of Technology, 2011, 18: 48−55.
[16] JU Shao-hua, TANG Mo-tang, YANG Sheng-hai, TANG Chao-bo. Thermodynamics of Cu(II)−NH_3−NH_4CI−H_2O system [J]. Transactions of Nonferrous Metals Society of China, 2005, 15(6): 1414−1419.
[17] WILLIAMSON A J, VERBRUGGEN F, RICO V S C, BERGMANS J, SPOOREN J, YURRAMENDI L, LAING G D, BOON N, HENNEBEL T. Selective leaching of copper and zinc from primary ores and secondary mineral residues using biogenic ammonia [J]. Journal of Hazardous Materials, 2021, 403: 123842.
[18] VELÁSQUEZ-YÉVENES L, RAM R. The aqueous chemistry of the copper−ammonia system and its implications for the sustainable recovery of copper [J]. Cleaner Engineering and Technology, 2022, 9: 100515.
[19] LIMPO J L, FIGUEIREDO J M, AMER S, LUIS A. The CENIM-LNETI process: A new process for the hydrometallurgical treatment of complex sulphides in ammonium chloride solutions [J]. Hydrometallurgy, 1992, 28: 149−161.
[20] LIU Wei, TANG Mo-tang, TANG Chao-bo, HE Jing, YANG Sheng-hai, YANG Jian-guang. Dissolution kinetics of low grade complex copper ore in ammonia−ammonium chloride solution [J]. Transactions of Nonferrous Metals Society of China, 2010, 20(5): 910−917.
[21] NABIZADEH A, AGHAZADEH V. Dissolution study of chalcopyrite concentrate in oxidative ammonia/ammonium carbonate solutions at moderate temperature and ambient pressure [J]. Hydrometallurgy, 2015, 152: 61−68.
[22] RAO K S, RAY H S. A new look at characterisation and oxidative ammonia leaching behaviour of multimetal sulphides [J]. Minerals Engineering, 1998, 11(11): 1011−1024.
[23] FENG D, van DEVENTER J S J. Leaching behaviour of sulphides in ammoniacal thiosulphate systems [J]. Hydrometallurgy, 2002, 63(2): 189−200.
[24] BECKSTEAD L W, MILLER J D. Ammonia, oxidation leaching of chalcopyrite-reaction kinetics [J]. Metallurgical Transactions B, 1977, 8: 19−29.
[25] WARREN G W, WADSWORTH M E. The electrochemical oxidation of chalcopyrite in ammoniacal solutions [J]. Metallurgical Transactions B, 1984, 15: 289−297.
[26] MOYO T, PETERSEN J, FRANZIDIS J P, NICOL M. An electrochemical study of the dissolution of chalcopyrite in ammonia–ammonium sulphate solutions [J]. Canadian Metallurgical Quarterly, 2015, 54(3): 269−278.
[27] MA Ya-long, YANG Yi, FAN Rong, GAO Xi-yu, ZHENG Lei, CHEN Miao. Chalcopyrite leaching in ammonium chloride solutions under ambient conditions: Insight into the dissolution mechanism by XANES, Raman spectroscopy and electrochemical studies [J]. Minerals Engineering, 2021, 170: 107063.
[28] NICOL M J. A comparative assessment of the application of ammonium chloride and glycine as lixiviants in the heap leaching of chalcopyritic ores [J]. Hydrometallurgy, 2018, 175: 285−291.
[29] BECKSTEAD L W, MILLER J D. Ammonia, oxidation leaching of chalcopyrite-surface deposit effects [J]. Metallurgical Transactions B, 1977, 8: 31−38.
[30] YIN Q, KELSALL G H, VAUGHAN D J, ENGLAND K E R. Atmospheric and electrochemical oxidation of the surface of chalcopyrite ($CuFeS_2$) [J]. Geochimica et Cosmochimica Acta, 1995, 59(6): 1091−1100.
[31] FORWARD F A, MACKIW V N. Chemistry of the ammonia pressure process for leaching Ni, Cu, and Co from Sherritt Gordon sulphide concentrates [J]. JOM, 1955, 7: 457−463.
[32] HUA Xiao-ming, ZHENG Yong-fei, XU Qian, LU Xiong-gang, CHENG Hong-wei, ZOU Xing-li, SONG Qiu-shi, NING Zhi-qiang. Interfacial reactions of chalcopyrite in ammonia–ammonium chloride solution [J]. Transactions of Nonferrous Metals Society of China, 2018, 28(3): 556−566.
[33] ANSAH E O, JYOTI A, BLACK J R, HAESE R R. The importance of reaction mechanisms and coupled dissolution with reprecipitation (CDR) reactions when modelling copper leaching in heap systems [J]. Minerals Engineering, 2023, 203: 108357.
[34] MOYO T, PETERSEN J. Study of the dissolution of chalcopyrite in solutions of different ammonium salts [J]. Journal of the Southern African Institute of Mining and Metallurgy, 2016, 116(6): 509−516.
[35] DUTRIZAC J E. Ammoniacal percolation leaching of copper ores [J]. Canadian Metallurgical Quarterly, 1981, 20(3): 307−315.
[36] SUN He-yun, RUAN Ren-man. Method of ammonia heapleach of copper sulphides: China Patent, 202310883860.3 [P]. 2023−09−11. (in Chinese)

[37] SHEN Zhi-hao, WEN Shu-ming, HAO Jia-mei, FENG Qi-cheng. Flotation separation of chalcopyrite from pyrite using mineral fulvic acid as selective depressant under weakly alkaline conditions [J]. Transactions of Nonferrous Metals Society of China, 2025, 35(1): 313−325.
[38] MENG Xing-hui, HAN K N. The principles and applications of ammonia leaching of metals—A review [J]. Mineral Processing and Extractive Metallurgy Review, 1996, 16(1): 23−61.
[39] ZHAO Chun-xiao, WANG Jun, LIU Yang, LIAO Rui, YANG Bao-jun, QIU Guan-zhou. Influencing mechanism of visible light and silver ions on p- and n-type chalcopyrite bioleaching [J]. Transactions of Nonferrous Metals Society of China, 2024, 34(2): 655−668.
[40] de FARIA D L A, LOPES F N. Heated goethite and natural hematite: Can Raman spectroscopy be used to differentiate them? [J]. Vibrational Spectroscopy, 2007, 45(2): 117−121.
[41] HANESCH M. Raman spectroscopy of iron oxides and (oxy) hydroxides at low laser power and possible applications in environmental magnetic studies [J]. Geophysical Journal International, 2009, 177(3): 941−948.
[42] TSHILOMBO A F. Mechanism and kinetics of chalcopyrite passivation and depassivation during ferric and microbial leaching solutions [D]. Vancouver, Canada: The University of British Columbia, 2004.
[43] BABA A A, GHOSH M K, PRADHAN S R, RAO D S, BARAL A, ADEKOLA F A. Characterization and kinetic study on ammonia leaching of complex copper ore [J]. Transactions of Nonferrous Metals Society of China, 2014, 24(5): 1587−1595.
[44] YIN Q, VAUGHAN D J, ENGLAND K E R, KELSALL G H, BRANDON N P. Surface oxidation of chalcopyrite ($CuFeS_2$) in alkaline solutions [J]. Journal of the Electrochemical Society, 2000, 147(8): 2945.
[45] NICOL E A, BARON J Y, MIRZA J, LEITCH J J, CHOI Y, LIPKOWSKI J. Surface-enhanced Raman spectroscopy studies of the passive layer formation in gold leaching from thiosulfate solutions in the presence of cupric ion [J]. Journal of Solid State Electrochemistry, 2014, 18: 1469−1484.
[46] BREUER P L, JEFFREY M I. The reduction of copper(II) and the oxidation of thiosulfate and oxysulfur anions in gold leaching solutions [J]. Hydrometallurgy, 2003, 70: 163−173.
[47] VELSO T C, PEIXOTO J J M, PEREIRA M S, LEAO V A. Kinetics of chalcopyrite leaching in either ferric sulphate or cupric sulphate media in the presence of NaCl [J]. International Journal of Mineral Processing, 2016, 148: 147−154.
[48] TANDA B C, EKSTEEN J J, ORABY E A, O'CONNOR G M. The kinetics of chalcopyrite leaching in alkaline glycine/glycinate solutions [J]. Minerals Engineering, 2019, 135: 118−128.
[49] NYEMBWE K J, FOSSO-KANKEU E, WAANDERS F, MKANDAWIRE M, NYEMBWE D K, MAMBA B B. Influence of Fe_3O_4 on redox changes during Cu dissolution from $CuFeS_2$ in acidified ferric sulfate [J]. Transactions of Nonferrous Metals Society of China, 2024, 34(6): 1965−1975.
[50] LIU Xin-Jie, LIAO Ya-long, LIU Qing-feng, WU Min. Influence of tartrate on leaching interface of low-grade polymetallic complex chalcopyrite ore [J]. Transactions of Nonferrous Metals Society of China, 2024, 34(12): 4049−4062.

控电位密闭条件下黄铜矿氨浸动力学

孙和云[1,2,3,4]，阮仁满[2,3]，邓久帅[1,4]

1. 中国矿业大学(北京) 化学与环境工程学院 有色金属行业三稀资源综合利用工程技术研究中心，有色金属行业共伴生资源分离加工重点实验室，北京 100083；
2. 中国科学院过程工程研究所 战略性金属资源绿色循环利用国家工程技术研究中心，北京 100190；
3. 中国科学院过程工程研究所 绿色过程与工程重点实验室，北京 100190；
4. 中国矿业大学(北京) 内蒙古研究院，鄂尔多斯 017001

摘 要：为了优化黄铜矿氨法堆浸工艺，采用密封搅拌反应装置，在常温、控制氧化还原电位条件下研究了黄铜矿氨浸动力学的关键因素。结果表明，氧化还原电位、粒度和 pH 对黄铜矿的浸出速率有显著影响。粒度和羟基离子浓度 $c(OH^-)$的反应级数分别为−2.39 和 0.55；温度在 25~45 ℃范围内对黄铜矿氨浸影响不显著；碳酸铵介质比氯化铵和硫酸铵介质更有利于黄铜矿浸出。氨浸渣表面沉积物以多孔氧化铁为主，主要为赤铁矿和水铁矿，对黄铜矿的浸出形成扩散阻碍。收缩核模型分析表明，黄铜矿氨浸第二阶段由产物层扩散控制，较低的活化能(10.18 kJ/mol)进一步证实了扩散控制机理。

关键词：黄铜矿；浸出动力学；氧化还原电位；氨浸出；表面沉积物

(Edited by Bing YANG)